Macromolecular Research, Vol. 13, No. 2, pp 152-155 (2005)

Unstable Inverted Phases of Di- and Tri-block Copolymers on Solution-Casting Films

Dachun Sun

Department of Educational Technology Baicheng Normal College, Baicheng, Jilin, 137000, P. R. China

Lei Huang and Haojun Liang*

Department of Polymer Science and Engineering, University of Science and Technology of China, Hefei, Anhui, 230026, P. R. China

Received January 5, 2005; Revised March 7, 2005

Abstract: A dynamic density functional theory is presented for the observation of the phase revolutions of a solution-casting film of di- and tri-block copolymers under solvent evaporation conditions. With the evaporation of the solvent, the inverted phases, the minor part of the component becomes the continuous phase at the higher solvent evaporation rate, as observed in this experiment. Further simulation revealed that these inverted phases are converted into the normal phase and the major part of the component becomes the continuous phase, implying that the inverted phases observed in this experiment are unstable.

Keywords: DDFT, phase separation, block copolymer, solution-casting film.

Introduction

Block copolymers, including linear and star block copolymers, have an ability to assemble into various complex periodic ordered microstructures.[1-8] Materials with those structures play a fundamental role in nano- or micro-scale manufacturing industry. In practice, such materials are usually generated through the solution-cast[9-12] from a co-solvent of each block. As acknowledged, the final microstructures should rely not only on the interactions between components[13] but also on the evaporation rate of solvents.[14-18] Recent experimental[14-17] and theoretical[18] observations on the solvent evaporation speed dependence of microstructures for block copolymers demonstrated that a complex phase evolution process exists. In particular, Zhang *et al.*[16] reported an inverted phase on solvent-induced order-disorder transition (ODT) studies of poly(styrene-butadiene-styrene) SBS triblock/diblocks, i.e. at a relative high solvent evaporation rate, the minority component [polystyrene in shorter block length] displays as a continuous phase and majority component [polybutadiene in longer block length] as dispersed phases. Very recently, Huang *et al.*[18] demonstrated that similar phase behaviors also exist in the SB diblock copolymer system. This remains an open question that if the inverted phase is in stable state? In this paper, we try to explore the issue by using dynamic-density functional theory methods developed for observation of microphase evolution during the evaporation of solvent.

*e-mail: sun_dachun@eyou.com
1598-5032/04/152-04

Modeling and Calculations

Instead of the detailed description of the dynamic mean-field density functional theory as given in references (18~20), only the main parts of the theory have been provided here. We employ freely jointed lattice chain model and more sophisticated model based on an off-lattice gaussian chain model. Supposing n linear block copolymer chains with N_A segments of type A, N_B segments of type of B (Length of the chain is $N = N_A + N_A$) and S solvents are involved in the volume V. On a coarse-grained time scale, there is a certain collective particle concentration field $\rho_I(r)$ of components I (A, B and S) at position r. Given this concentration field, a free-energy functional $F[\rho]$ is defined as follows:

$$F[\rho] = -\beta^{-1} n \ln \Phi + \beta^{-1} \ln n! - \sum_I \int U_I(r) \rho_I \, dr + F^{nid}[\rho] \quad (1)$$

where Φ is the partition functional for a freely jointed chain in the external field U_I, and $F^{nid}[\rho]$ is the contribution from nonideal interactions. The free-energy function derives from an optimization criterion which introduces the external potential field U_I as a lagrange multiplier field. The

relation between the external potential and the concentration field is bijective and given by a density functional freely jointed chains:

$$\rho_I[U](r) = \sum_{K=1}^{n}\sum_{s=1}^{N} \delta_{Is}^{K} Tr_c \psi\delta(r-R_s) \tag{2}$$

δ_{Is}^{K} is a Kronecker delta function with value 1 if bead s is of type I and 0 otherwise. ψ is the single chain configuration distribution function

$$\Psi = \frac{1}{\Phi} e^{-\beta\left[H^{id} + \sum_{s=1}^{N} U_s(r)\right]} \tag{3}$$

where H^{id} is an Edwards' connectivity Hamiltonian for the constant bond length freely jointed chain model

$$\exp -\beta H^{id}(R_1, \ldots, R_N)\prod_{s=2}^{N}\delta(|R_s - R_{s-1}| - a) \tag{4}$$

where a is the bond length.

The intrinsic chemical potential $\mu_I(r)$ is expressed as follows:

$$\begin{aligned}\mu_I(r) = -U_I(r) + \sum_J \int_V \varepsilon_{IJ}(|r-r'|)\rho_J(r')dr' \\ + k_H v_I \sum_J \int_V v_J \rho_J(r)\end{aligned} \tag{5}$$

where the unimportant constant term $\sum_J v_J \rho_J^0$ is omitted. In equilibrium $\mu_I(r)$ is constant, this yields the familiar self-consistent field equations for freely jointed chains model. When the system is not in equilibriumthe gradient of the intrinsic chemical potential $-\nabla\mu_I$ acts as the thermodynamic force which drives collective relaxation processes. When Onsager coefficients are constant, the local flux:

$$J_I = -M\nabla\mu_I + \tilde{J}_I \tag{6}$$

where M is mobility coefficient, $\tilde{J}_I$ is a flux arising from thermal fluctuations. Together with the continuity equation

$$\frac{\partial\rho_I}{\partial t} + \nabla\cdot J_I = 0 \tag{7}$$

we find bare functional Langevin equation of the simple diagonal form:

$$\frac{\partial\rho_I(r)}{\partial t} = \nabla\cdot M\nabla\mu_I + \eta_I \tag{8}$$

with the distribution of the noise η_I according to the fluctuation dissipation theorem:

$$\langle \eta_I(r,t)\rangle = 0 \tag{9}$$

$$\langle \eta_I(r,t)\eta_J(r',t')\rangle = -2M\beta^{-1}\delta(t-t')\times\nabla\cdot\delta(r-r')\rho_I\nabla_{r'} \tag{10}$$

The density patterns of quenched block copolymer melt depicted in the study were obtained by numerical integration of the diffusion equation (eq. 8) on the cubic mesh through Crank-Nicolson scheme. In this calculation strategy, the freely jointed chain densities function of the I-type segments, $\rho_I[U](r)$, can be expressed in terms of Green function as follows:

$$\rho_I[U](r) = \frac{n}{\Lambda^3\Phi}\sum_{s=1}^{N}\delta_{Is}^{K} G_s(r)\sigma[G_{s+1}^{i}](r), \tag{11}$$

where the Green function, $G_{k,s}(r)$, and inverse Green function, $G_{k,s+1}^{i}(r)$, of chain can be calculated by once-integrated Green propagators schemed as following:

$$G_0(r) = G_{N+1}^{i} = 1 \tag{12}$$

$$G_K(r) = e^{-\beta U_K(r)}\sigma[G_{K-1}](r) \tag{13}$$

$$G_K^{i}(r) = e^{-\beta U_K(r)}\sigma[G_{K+1}^{i}](r) \tag{14}$$

the delta connectivity operator defined by

$$\sigma[X](r) = \frac{1}{4\pi a^2}\int_V \delta(|r-r'|-a)\cdot X(r')\cdot\, dr' \tag{15}$$

and can be calculated on grid lattice space based upon the strategies of Fraaije.[19] The simulation was performed in a *true* 2D lattice algorithm to be more trackable in computatation time and easier in visualization. After Fraaije's work[19]

$$\begin{aligned}\sigma[X](x,y) = \frac{1}{4}[X(x-1,y) + X(x+1,y) \\ + X(x,y-1) + X(x,y+1)\end{aligned} \tag{16}$$

the central terms in eq. A6 and A7 in ref. (19) had been omitted, which is reasonable as indicated by Fraaije.

In order to control the solvent evaporation rate, the thin film was placed in a container with a small opened hole in the ceiling as the experimental description in ref. (16). The volume reduction of the solvents through the opened hole per successive time will be calculated based on the following equation (see Appendix in ref. (18)):

$$\Delta V = \frac{A'Bc_s}{c_s + B(c_s + c_p)} \tag{17}$$

where c_s and c_p are the instantaneous volume fractions of the solvent and the copolymer, respectively, A' is a parameter correlated to the natural properties of solvents and B is a parameter proportional to the area of the opened hole, i.e. the solvent evaporation rate can be controlled through the adjustment of the value of B. Hence, in the numerical simulation process the average concentration of each compo-

nent, $\overline{\rho}_i$, varies following the solvent evaporation and the density of component i at position r, $\rho_i(r)$, calculated in terms of eq. (11). Based on the above procedures the influence of solvent evaporation on the microdomain structures of block copolymers is investigated.

Results and Discussion

The simulations are performed on a 2D square with 25 × 25 grids. The volume fractions of B block for di- and triblock copolymers are $f_B = 0.23$ and $f_B = 0.29$ respectively. The interaction parameters between different components are assigned respectively to $\chi_{AB} = 6.25, \chi_{SA} = 1.75, \chi_{SB} = 0.50$, $\chi_{AA} = \chi_{BB} = \chi_{SS} = 0.0$, indicting that blocks A and B are immiscible and the solvent is preferential to short block. Figure 1 shows the evolution of the microstructures as the function of concentrations in the BAB triblock copolymer solution in the case of a high solvent evaporation rate, that is accomplished through assigning the value of parameters $A' = 0.16$ and $B = 1.0$ in the eq. A8 in ref. (18). Because of the preference of the solvent to the short block B the short blocks B together with solvents are majority components, and form a continuous phase, then the long block A forms dispersed phases [Figure 1(a)]. Because of the viscosity behaviors and entanglement effect of macromolecular chains the relaxation time of such molecules may become longer than the evaporation time of solvents if the evaporation rate of the solvent is sufficient high. Thus, as shown in Figure 1(b)-(d) the phases comprising longer blocks A appear as dispersed phases even the solvents in the system are almost drained [Figure 1(d)]. As a result, the minority components comprising block B are in continuous phase. The inverted phase reported by Zhang *et al.*[16] is also theoretically observed here. However, further observation of the change of micro-phase morphologies reveals that these inverted phases are unstable. As shown in Figure 1(e) and (f), they finally converted into regular phase patterns, in which the minority component [block B] is dispersed phases. We also carry out the observation in the A-B diblock copolymers system, similar result is also obtained, as shown in Figure 2. Consequently, we can conclude that the inverted phases observed by Zhang *et al.*[16] are metastable states being frozen by the fast evaporation processes. Inspired by the experiment work of Kim *et al.*,[14] we suppose that post-evaporation annealing of inverted phase would lead to a regular microphase morphology, a more stable state.

Conclusions

The phase revolutions of the solution-casting film of di-

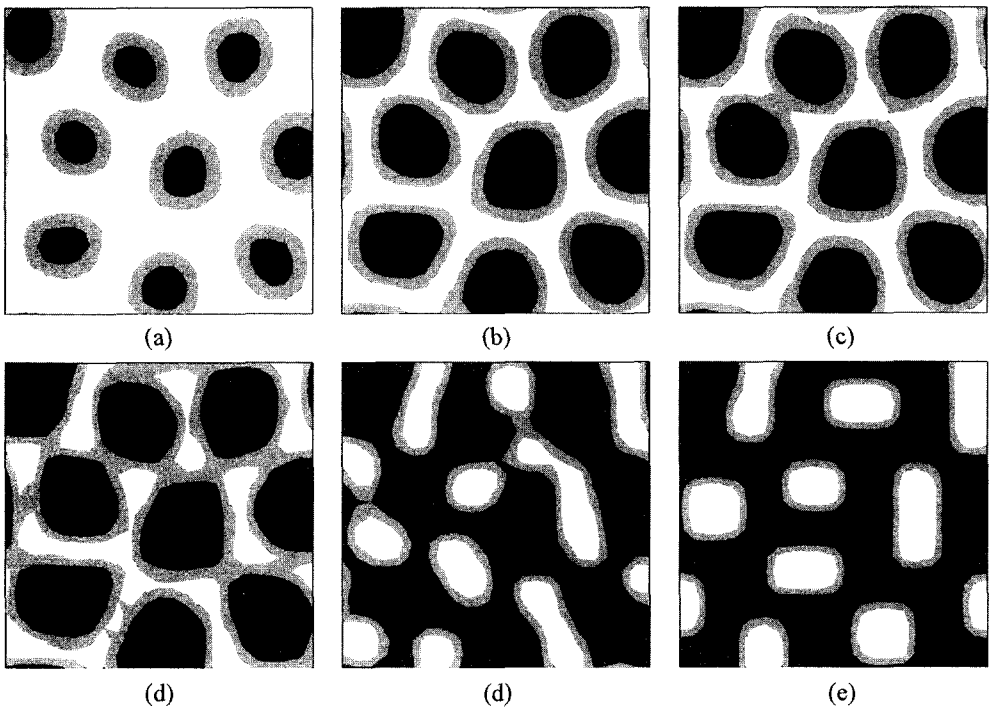

Figure 1. Microdomain patterns of B-A-B triblock coplymer ($f_B = 0.29$) solution at different polymer volume fractions during the evaporation process with parameter $A' = 0.16$ and $B = 1.0$. (a)~(f) corresponding to cases of polymer volume fractions 0.426, 0.831, 0.873, 0.983, 1.000 and long time after all solvents are drained respectively. Different colors are corresponding to different density region. Black, gray and white indicate density of component A between (0.7, 1.0), (0.3, 0.7) and [0.0, 0.3]. We used linear interpolation instead of smoothing in visualization. All figures in Figures 1~2 are in the same style.

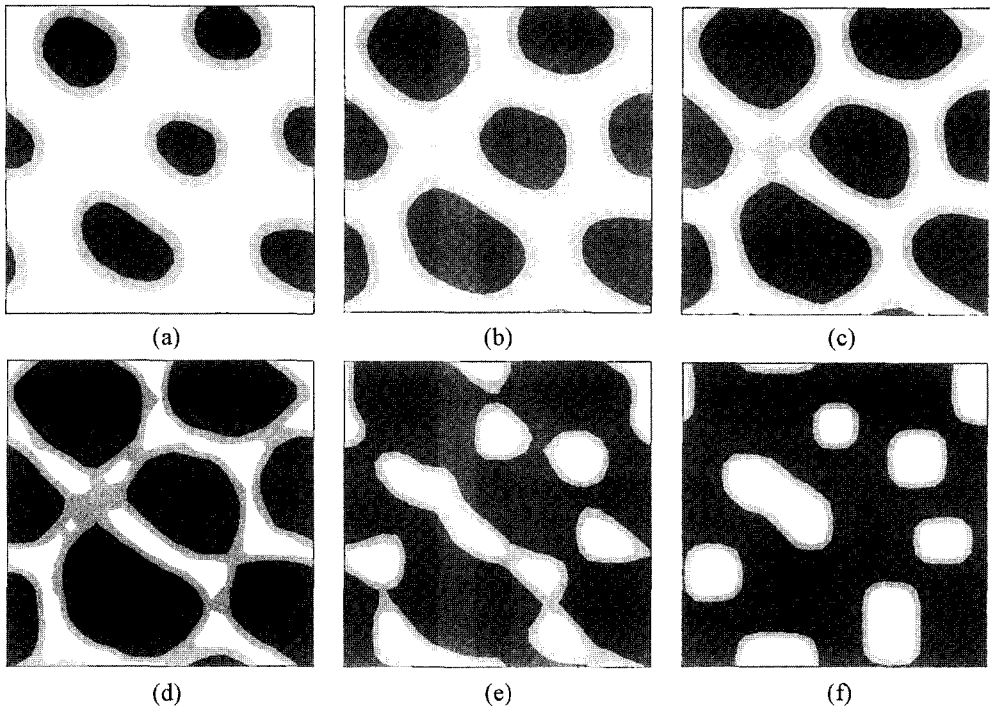

Figure 2. Microdomain patterns of A-B diblock coplymer (f_B = 0.23) solution at different polymer volume fractions during the evaporation process with parameter A'=0.16 and B=1.0. (a)~(f) corresponding to cases of polymer volume fractions 0.400, 0.688, 0.831, 0.983, 1.000 and long time after all solvents are drained respectively.

and triblock copolymers under solvent evaporations have been observed by the Dynamic Density Functional Field theory. Indeed, we observed the inverted phases, the minor part of the component became the continue phase, at the higher solvent evaporation rate, as observed in experiment.[16] Further simulation revealed that these inverted phases convert into the normal phase patters, the major part of the component becomes continue phase, implying the inverted phases observed in experiment[16] are in the unstable state. They can be observed in experiment simply because of the low motion ability of the macromolecule chain in melt.

References

(1) F. S. Bates and G. H. Fredrickson, *Annu. Rev. Phys. Chem.*, **41**, 525 (1990).
(2) K. Mortensen, *Curr. Opin. Colloid Inter. Sci.*, **3**, 12 (1998).
(3) C. Y. Wang and T. P. Lodge, *Macromolecules*, **35**, 6997 (2002).
(4) T. P. Lodge, B. Pudil, and K. J. Hanley, *Macromolecules*, **35**, 4707 (2002).
(5) Y. Termonia, *J Polym. Sci. Polym. Phys.*, **40**, 890 (2002).
(6) S. Burke, H. W. Shen, and A. Eisenberg, *Macromolecular Symposia*, **175**, 273 (2001).
(7) M. Maskos and J. R. Harris, *Macro. Rap. Comm.*, **22**, 271 (2001).
(8) F. S. Bates and G. H. Fredrickson, *Phys. Today*, **52**, 32 (1999).
(9) L. H. Radzilowski and S. I. Stupp, *Macromolecules*, **27**, 7747 (1994).
(10) S. J. M. Yu, C. M. Soto, and D. A. Tirrell, *J. Am. Chem. Soc.*, **122**, 6552 (2000).
(11) S. Ludwigs, A. Boker, A. Voronov, N. Rehse, R. Magerle, and G. Krausch, *Nat. Mater.*, **2**, 744 (2003).
(12) S. H. Kim, M. J. Misner, T. Xu, M. Kimura, and T. P. Russell, *Adv. Mater.*, **16**, 226 (2004).
(13) F. S. Bates, *Science*, **251**, 898 (1991).
(14) G. Kim and M. Libera, *Macromolecules*, **31**, 2569 (1998).
(15) H. G. Jeon, S. D. Hudson, H. Ishida, and S. D. Smith, *Macromolecules*, **32**, 1803 (1999).
(16) Q. L. Zhang, O. K. C. Tsui, B. Y. Du, F. J. Zhang, T. Tang, and T. B. He, *Macromolecules*, **33**, 9561 (2000).
(17) H. Y. Huang, F. J. Zhang, Z. J. Hu, B. Y. Du, T. B. He, F. K. Lee, Y. J. Wang, and O. K. C. Tsui, *Macromolecules*, **36**, 4084 (2003).
(18) L. Huang, X. H. He, T. B. He, and H. J. Liang, *J. Chem Phys.*, **119**, 12479 (2003).
(19) J. G. E. M. Fraaije, *J. Chem. Phys.*, **99**, 9202 (1993).
(20) J. G. E. M. Fraaije, B. A. C. Van Vlimmeren, N. M. Maurits, M. Postma, O. A. Evers, C. Hoffmann, and G. Goldbeck-Wood, *J. Chem. Phys.*, **106**, 4260 (1997).